Journal of the Korean Nuclear Society
Volume 31, Number 1, pp.88~103, February 1999

Post Test Analysis of the Phebus FPT1 Experiment

Song Won Cho, Jong Hwa Park, and Hee Dong Kim
Korea Atomic Energy Research Institute
150 Dukjin-dong Yusong-gu, Taejon 305-353, Korea

(Received July 6, 1998)

Abstract

The purposes of this study are to understand the severe accident phenomena, to establish the simulation method for the experimental test, and to assess the current models in MELCOR for future improvement.

This paper presents the results of the PHEBUS FPT1 post test analysis using MELCOR computer code, version 1.8.4. The entire PHEBUS facility has been modeled; the core, the primary circuit including the steam generator, and the containment vessel. Both the thermal hydraulic and the fission product behavior have been investigated.

The code simulation results of the thermal hydraulic behavior show good agreement with the experimental data. The fission product release and transport are calculated using the CORSOR models in MELCOR code and the results will be compared with the experiment when the experimental data are available.

1. Introduction

This paper describes the results of the PHEBUS FPT1 [1,2] post test analysis using MELCOR computer code [3]. The entire PHEBUS facility has been modeled ; the core, the primary circuit including the steam generator, and the containment vessel. Both the thermal-hydraulic and the fission products behavior have been investigated.

The PHEBUS FP research program [4,5] is supported by the Nuclear Safety and Protection Institute (IPSN) of the Commissariat a l' Energie Atomique (CEA) and the Commission of the European Communities (CEC). This program consists of a series of in-pile tests performed in the PHEBUS experimental reactor at Cadarache Nuclear Center. The tests are conducted in close collaboration with United State, Canada, Japan and Korea.

The objectives of the PHEBUS FP program are to improve the understanding of physical phenomena occurring during a severe accident in a Pressurized Water Reactor (PWR) ; (a) core heat-up, (b) cladding burst and oxidation, (c) fuel damage and material relocation, and (d) fission products (FP) release, transport and deposition in the primary circuit and containment.

The PHEBUS FP program consists of 6 experiments as shown in Table 1. PHEBUS FPT1 which is the second test of the program was performed on July 26th, 1996 under similar experimental condition as for FPT0 [6] but with pre-irradiated fuel. The test requirements were; (a) Conditions of steam starvation in the bundle should be avoided, (b) FPs releases should be maximized, (c) FPs deposition along the unheated part of the upper plenum just above the bundle should be avoided, and (d) A limited amount of fuel (~20%) should be melted during the high temperature phase of the test.

MELCOR code is a fully integrated, engineering-level computer code that models the progression of severe accidents in Light Water Reactor (LWR) nuclear power plants. MELCOR code has been developed at Sandia National Laboratories (SNL) for the U.S. Nuclear Regulatory Commission (USNRC) as a second-generation plant risk assessment tool and the successor to the Source Term Code Package (STCP). The spectrum of severe accident phenomena, including reactor coolant system and containment thermal-hydraulic response, core heat-up, degradation and relocation, and fission product release and transport, is treated in MELCOR code in a unified frame work for both boiling water reactors and pressurized water reactor. MELCOR is used for BWR and PWR Probabilistic Risk Assessment (PRA), audit reviews of the Individual Plant Examination (IPE) submittals for American power plants, studies to develop insights into phenomena and hardware performance, and accident management studies.

The latest version of MELCOR code, 1.8.4QL, which was released on March 1998 and is run on a DEC Alpha 600 platform with operating system ULTRIX, has been used for the calculations described in this paper. The experimental results presented in this paper represent data available as of May 1998. Up to this date, the experimental data of the thermal-hydraulic behavior are released in electronic form [7], but only a restricted amount of the FP and aerosol data can be obtained in graphical form in reference 1. For this reason, a comparison of calculated results with experimental data has been made only for the thermal-hydraulic behavior of the test bundle and the containment.

Table 1. Planning of PHEBUS FP Test.

Test	Plan	Identification
FPT 0	Performed (Dec.1993)	Fresh fuel in oxidizing environment
FPT 1	Performed (July 1996)	Pre-irradiated fuel in oxidizing environment
FPT 4	June. 1999	Debris bed heat-up and melt
FPT 2	Nov. 1999	Pre-irradiated fuel in reducing environment
FPT 3	Oct. 2000	Open test
FPT 5	April 2002	Air ingress

2. Facility and Test Description

Facility : A schematic drawing of the facility for the PHEBUS FPT1 test is shown in Fig. 1. A more detailed description of the facility can be found in reference 8 and 9. The test bundle shown in Fig. 2 is located in a severe fuel damage (SFD) loop in the center part of the PHEBUS driver core which supplies the nuclear power. The fuel rods in the test bundle are 1.13 m long with a 1 m long fissile zone. The rods are held in place by two zircaloy spacer grids and are arranged in a 5x5 square lattice with the corner rods removed. One PWR control rod (Ag-In-Cd) is located in the center of the bundle, with a zircaloy guide tube. The rods are cooled by the steam entering at the bottom of the test section.

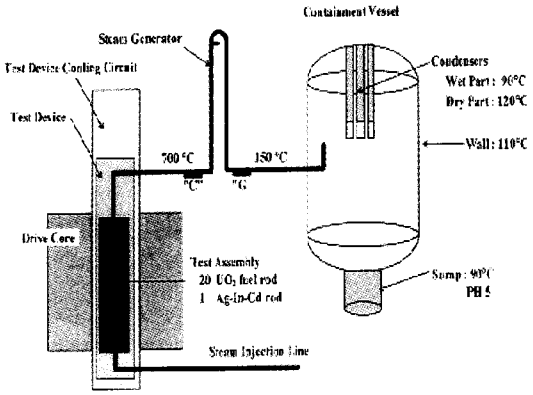

Fig. 1. Schematic Presentation of the PHEBUS FPT1 Test Facility (from ref.8)

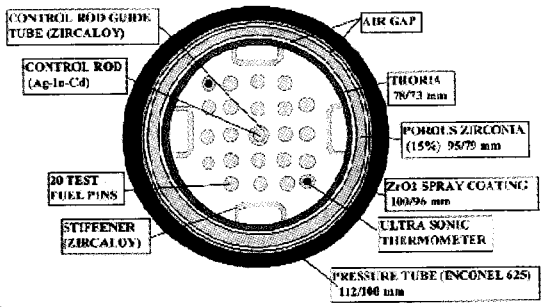

Fig. 2. Radial Cross-section of the PHEBUS FPT1 Test Bundle (from ref.8)

The test bundle is surrounded by an insulating zirconia shroud with an inner circular ThO_2 layer. Four zircaloy stiffeners are positioned on the inside surface of the shroud facing the fuel rods. The shroud is surrounded by an external ZrO_2 layer and a pressure tube of inconel coated on the internal surface by a spray of dense ZrO_2. These three annular structures are separated by two gaps in cold conditions. The outer pressure tube is cooled by an independent cooling circuit.

The two fresh fuel rods, control rod, stiffeners and shroud are equipped with thermocouples (TC) to control the thermal behavior of the test bundle during the experiment. More detailed information on the design and the instrumentation of the test bundle are available in reference 8.

During the experiment, the fuel bundle of the test facility is heated up by fission power induced by the driver core which surrounds the test bundle. The heat-up rate is representative for a severe accident. The fuel bundle temperatures becomes sufficiently high to cause core degradation, and fission products are released in gaseous or particulate form. The released fission products are then transported with a flow of steam and hydrogen through the primary circuit and eventually to the containment vessel. The containment vessel contains 3 condensers which are divided into two parts; a dry condenser and a wet condenser.

Two instrumentation groups are provided; one located before the steam generator at point C and the another after the steam generator at point G in Fig.1. Gas and aerosol composition, particle size distribution, deposited mass, and composition of the deposits are measured at these two locations.

Test : The FPT1 experiment is the second one of the six experiments planed and was executed on 26 July 1996. The most important difference between FPT0 and FPT1 is the burn-up of the fuel rods; fresh fuel was used in FPT0, while pre-irradiated fuel was used in FPT1. The fuel rods in FPT1, therefore, contain significantly higher fission product inventory.

The general characteristics of the FPT1 experiment [9,10] are based to some extent on a small or intermediate break LOCA scenario. The primary system is depressurised to 0.2 Mpa and the fission product chemistry takes place under oxidizing conditions.

The total duration of the FPT1 experiment is about 18,000 sec. The first phase so-called pre-transient phase of about 8,000 sec is followed by

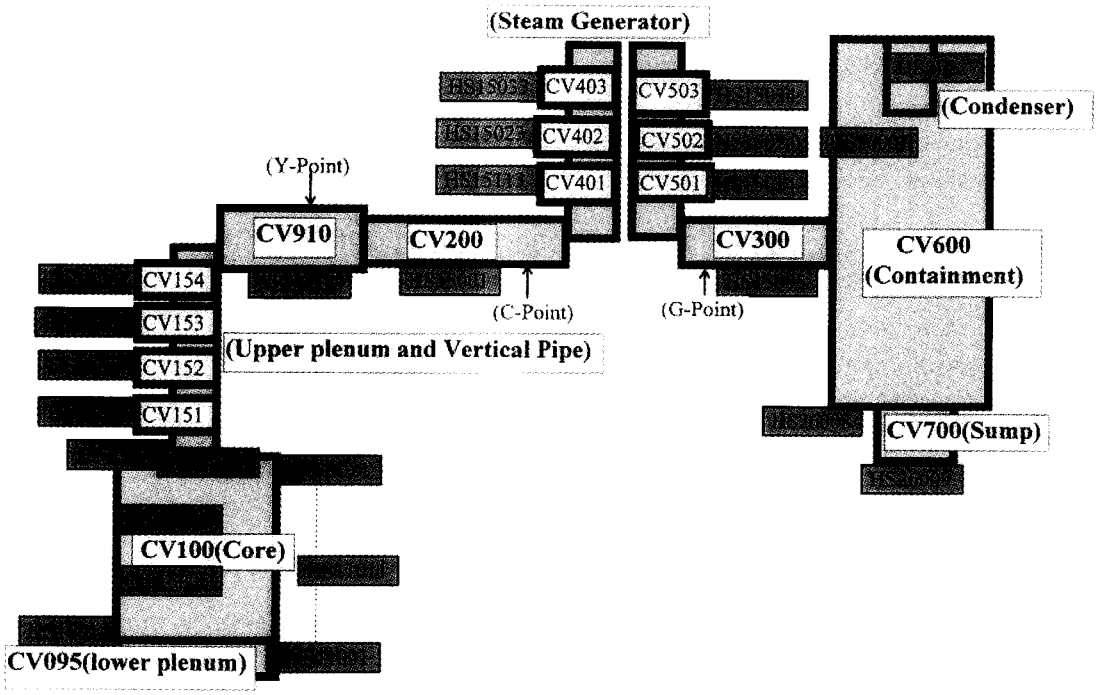

Fig. 3. MELCOR Nodalization of the FPT1 Test Facility

the transient phase which lasts for about 10,000 sec. The pre-transient phase is the thermal calibration phase of the bundle and some core degradation starts in this phase. The major part of the core degradation takes place in the transient phase.

3. Input Description

3.1. System Nodalization

Thermal-hydraulic behavior is modeled in MELCOR code in terms of control volumes and flow paths. The control volume is characterized by pressure and temperature. All hydrodynamic material and its energy reside in control volumes. Hydrodynamic material includes the coolant and non-condensable gases. These materials are assumed to be separated under the influence of gravity. The control volumes are connected by flow paths through which the hydrodynamic materials may move without residence time. Based on the elevations of the pool surfaces in the connected control volumes relative to the junctions with the flow paths, both pool and atmosphere may pass through each flow path.

The FPT1 nodalization scheme consists of 17 control volumes as shown in Fig. 3. The control volumes are modeled ; (a) in front of the core, an inlet volume is modeled in which the steam is injected, (b) the vertical pipe above the core is divided into four control volumes and the steam generator is divided into six control volumes, because there are large temperature gradient between gas and wall, (c) the horizontal pipe before the steam generator is modeled as two control volumes and the cold leg is modeled as one control volume, (d) the containment vessel

and the sump are modeled as one control volume each. The total 17 control volumes are connected by 16 flow paths. The total number of heat structures is 46, and 25 of them are required for the modeling of the core. The more detailed geometrical data can be found in reference 8.

3.2. Core Modeling

The MELCOR COR package calculates the thermal response of the core and lower plenum structures. In addition, the relocation of core materials during melting, slumping, and debris formation are modeled. Cell is the basic nodalization unit in the COR package. All important heat transfer processes are modeled in each cell. Thermal radiation within a cell and between different cells in both axial and radial directions are accounted for, as well as radiation to boundary structures and to liquid pool. The MELCOR COR Package needs extensive user input. Some important inputs used in this calculation are described below.

Core nodalization : The core is divided into 21 axial levels and two radial rings as shown in Fig. 4. All fuel rods are located in a single radial ring, because the core is very slender. The inner ring contains the control rod (Ag-In-Cd), cladding (Stainless steel), guide tube (zircaloy), and zircaloy grid spacers and the outer ring contains the fuel, cladding (zircaloy), zircaloy grid spacers. The lowest and highest levels do not contain fuel. The fuel part of the core is modeled by 19 levels in order to compare with experimental data, and the core inventory is determined by the data from reference 8.

The shroud surrounding the core bundle is represented by 21 heat structures corresponding to the core cell. The inner diameter of these heat structures is 73 mm. The inside liner of the shroud is a 2.5 mm layer of thoria, surrounded by

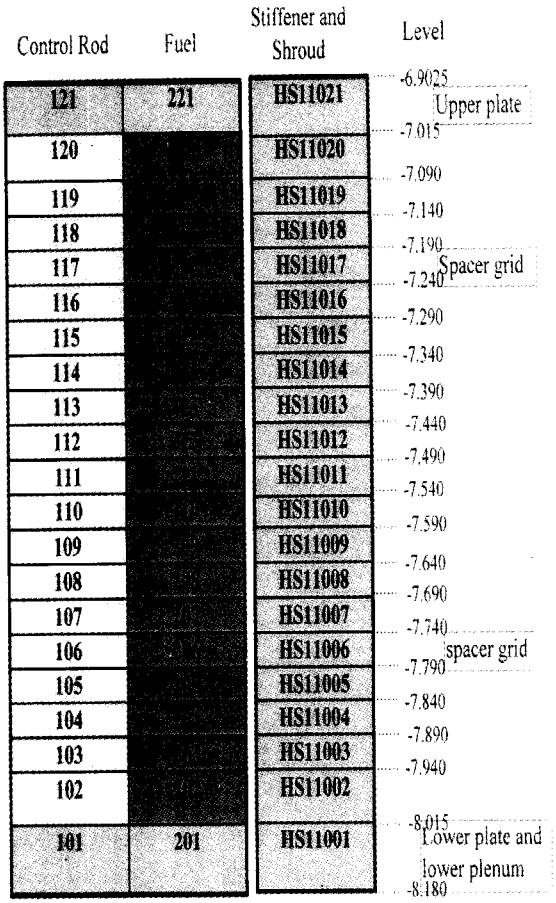

Fig. 4. MELCOR Nodalization of the Core

an air gap (0.5 mm), zirconia/yttria (8 mm), an air gap (0.5 mm), zirconia spray coating (2 mm), and Inconel (6 mm). Each heat structure communicates thermally with an axial level of the core at the same height.

Oxidation : Oxidation of zircaloy and steel is modeled for both the limiting cases of solid state diffusion of oxygen through the oxide layer, and gaseous diffusion of steam or oxygen through the mixture. Hydrogen is produced by oxidation of zircaloy and steel by steam. Oxidation takes place, only if the zircaloy or steel temperature is above 1,000 K (default; 1,100 K). However, the oxidation rate is very small at temperature below

1,200 K. A strong increase of the oxidation rate, a runaway, of zircaloy occurs at temperatures above 1,853 K. There is no runaway for steel.

Degradation criteria : The core degradation model treats eutectic reactions that lead to liquefaction several hundred degrees below normal melting points, dissolution reactions that lead to significant fuel relocations well below the UO_2 melting temperature, candling of molten core materials, and the deformation and relocation of particulate debris.

The cladding bursts if a temperature criterion is exceeded. The cladding failure temperature is taken as MELCOR default value of 1,173 K. The mechanical strength for hold-up of the fuel pellets is preserved, even if a gap release occurs.

There are two kind of core component failure options. Either is that the fuel rod is converted to particulate debris when remaining thickness of unoxidized zircaloy in the cladding fell below the user defined value, or the fuel rod can be held by the oxidized zircaloy until the temperature reaches the user input value. The temperature to which oxidized fuel rod can stand in the absence of unoxidized zircaloy in the cladding is set to 2,500 K (default is 2,800 K) which is the approximate melting temperature of the UO_2/ZrO_2 eutectic, and the temperature at which a fuel rod fails regardless of composition of cladding is given 3,100 K as default value which is the approximate melting temperature of UO_2. An intact component is converted to particulated debris whenever corresponding support of that component is lost.

Material Properties : The default values of material properties in MELCOR code or recommended values in reference 8 are used except for the conductivity of ZrO_2 (zirconia/yttria) and an air gap in the shroud. The ZrO_2 conductivity has large uncertainty and the result of pre-calculation needs about 10% higher conductivity in the range from 500 K to 1,500 K. The air gap is deformed during the test[11] and it is assumed that the gap disappeared above 700 K by the expansion.

3.3. Fission Product Release Modeling

MELCOR calculates both the release and transport behavior of fission products and control rod materials. It tracks the masses of these materials by 12 material classes. Each material class represents a group of one or more elements or compounds with similar physical properties. Each class has its own set of values of important parameters, such as release coefficients and vapor pressure. Fission product release takes place in two phases ; gap release and fuel heat-up. A small fraction of the volatile fission product species resides in the fuel-cladding gap during normal reactor operation [12,13]. If the cladding fails, all fission products residing in the gap are released. The larger part of the fission product release occurs due to the fuel heat-up. Three MELCOR options are available for the release of radionuclides from the fuel ; the CORSOR, CORSOR-M and CORSOR-Booth models. These release models are developed for release from fuel. Therefore, they are in principle not applicable to calculate the release of control rod poison.

The CORSOR model with default values for release rate coefficients and the surface-to-volume correction is used for this calculation. For the release of control rod materials, there is no suitable model in the code, so the CORSOR release model for the fuel is also applied.

In this calculation, it is assumed that Cs (class 2) and I (class 4) react to form CsI (class 16), if Cs and I are released at the same time. In general, Cs is in excess compared to I, which means that all mass in MELCOR class 4 reacts with a part of

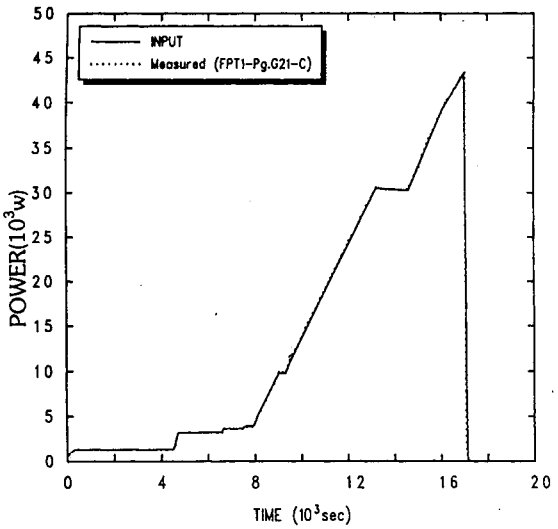

Fig. 5. History of the Bundle Power

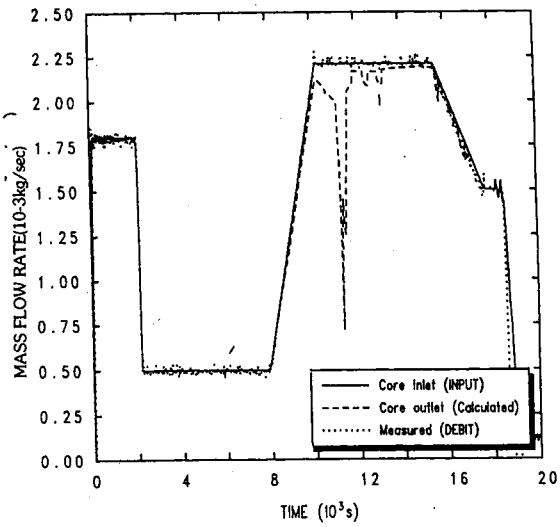

Fig. 6. Mass Flow Rates of the Steam at Core Inlet and Outlet

class 2 in order to form class 16. Consequently, all iodine is released as CsI and the mass of class 4 is negligible.

The aerosol dynamics portion of MELCOR code is based on the MAEROS computer program, except for the condensation model. MAEROS is a multicomponent aerosol dynamics code which evaluates the dynamic particle size distribution of each component. The dynamic size distribution is calculated between user defined minimum and maximum diameters. This range is subdivided into the user defined number of sections.

Aerosols and vapors are transported between control volumes by bulk fluid flow of the atmosphere and the pool, assuming zero slip. In addition, aerosols may settle from one control volume to a lower control volume in the absence of bulk flow.

Both agglomeration and deposition effects are included in MAEROS. Agglomeration of aerosols by Brownian motion, gravity, and turbulence is accounted for. The deposition processes are ; gravity, Brownian diffusion, thermophoresis, and diffusiophoresis. The hygroscopic effects and the Kelvin effect, which may play an important role for aerosol behavior in saturated or nearly saturated conditions, are also modeled in MELCOR code. The code, however, is not able to model the aerosol deposition by the inertia in the bends and at obstacles, and the deposited aerosols on the various surfaces cannot be resuspended. If a water film drains from a heat surfaces to the pool in the associated control volume, fission products deposited on that surface are relocated with the water.

It is found that the hygroscopic model is not adequate in the current version, and therefore is not used in this calculation. Consequently, the results show higher airborne aerosol concentration in the containment. This hygroscopic model will be examined after the model improvement.

3.4. Initial and Boundary Condition

The initial and boundary conditions are deduced from the experimental data [7] and the experimental procedure [9]. The power history generated in the fuel rods of the FPT1 core is shown in Fig. 5 with the input data , and the mass flow rate of the steam at the core inlet and outlet are shown in Fig. 6.

During the experiment, the temperatures of the riser and the horizontal line representing the upper plenum and hot leg are controlled to 973 K. The inside gas temperatures of the steam generator and cold leg are cooled down to 423 K. The initial conditions in the containment vessel are ; pressure 2.08 bar, gas temperature 369 K, relative humidity 90 % (instead of measured value of 64 %), gas composition 95 % nitrogen and 5 % oxygen. The temperatures of the condenser are set between 366 K to 364.6 K according to the experimental data.

4. Calculation and Results

4.1. Thermal Hydraulic Behavior

Temperature of core components : Due to the power produced in the core, the fuel rods are heated and temperatures start to rise. The fuel rods heat the control rod, the shroud, and the other structures by radiation between core components, radiation via steam, and convection. Table 2 provides major chronology of the events simulated by MELCOR code. Some calculated temperatures of core components are shown in Fig. 7 to 11 with the measured data. The calculated cladding rupture time (8,333 sec) is much later than the observed value in the experiment (5,800 sec), but the rupture temperature is predicted very well. The delayed

Table 2. Major Chronology of the Core Degradation

Phenomenon	Experiment	Calculation
Cladding rupture	5,800 sec	8,333 sec
Control rod rupture (start to relocation)	10,500sec	10,640 sec
Cladding oxidation		
Start	-	5,175 sec
Runaway	11,000-11,300sec	11,000- 11,500sec
Peak	11,260 sec	11,280 sec
Fuel relocation (start)	15,800 sec	15,560 sec
Total hydrogen generation	96 g	97 g

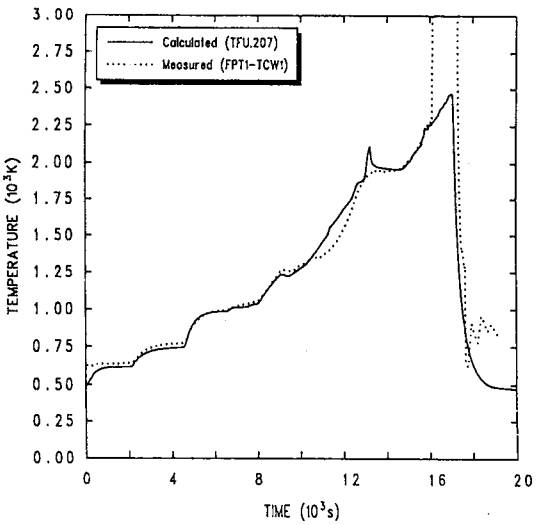

Fig. 7. Temperatures of the Fuel Rod at Level 30cm

predicted rupture time is due to the fact that the fuel temperature is almost constant in the range from 4,500 sec to 8000 sec during the thermal calibration phase as shown in Fig. 7 and 8. At temperature of 1,853 K, the temperature increase of the cladding accelerates, due to the strong increase of the oxidation rate of zircaloy above this temperature. Some measured fuel temperatures fluctuated above 2,300 K due to failure of the TC at about 13,000 sec, or due to relocation of core materials from the upper cell.

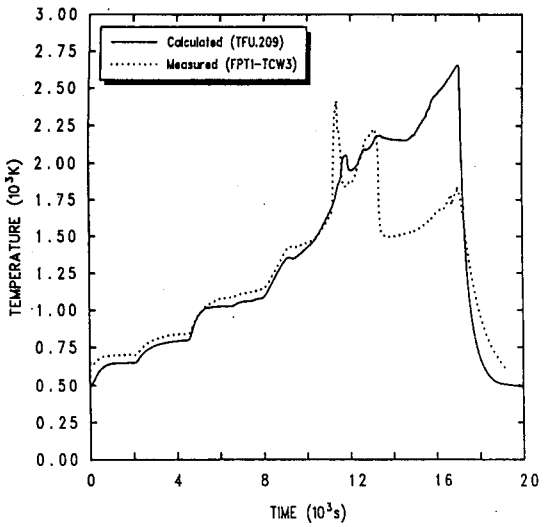

Fig. 8. Temperatures of the Fuel Rod at Level 40 cm

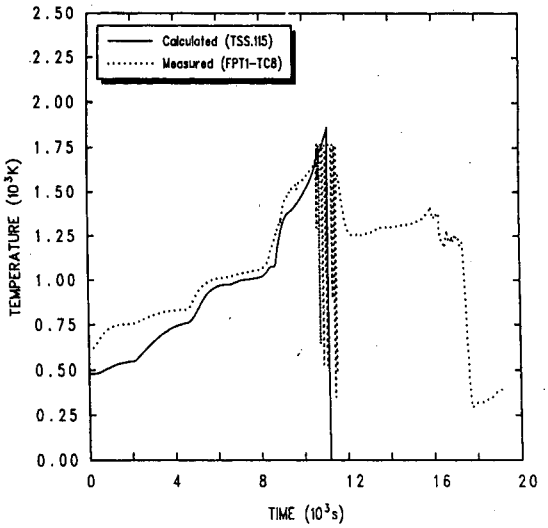

Fig. 9. Temperatures of the Control Rod at Level 70 cm

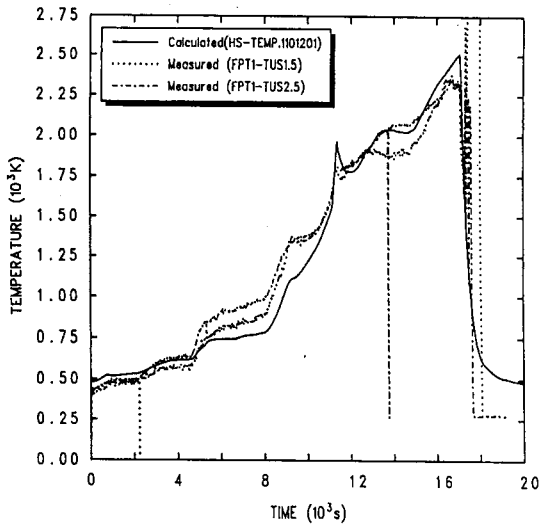

Fig. 10. Temperatures of the Channel Fluid at Level 51 cm

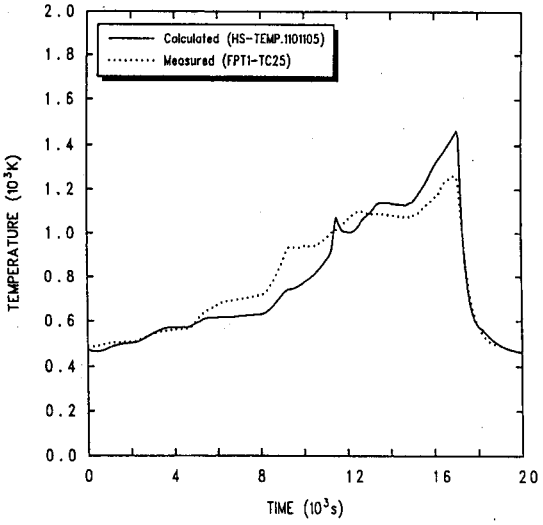

Fig. 11. Temperatures of the Outside Shroud at Level 50 cm

The temperature of a component suddenly drops to 0 K, which means that the component in the particular cell is removed by the relocation.

Hydrogen generation : Hydrogen is produced from the oxidation of zircaloy and steel by steam. The hydrogen production rate and the cumulative mass are shown in Fig. 12. The total hydrogen production is 97 g, which is good

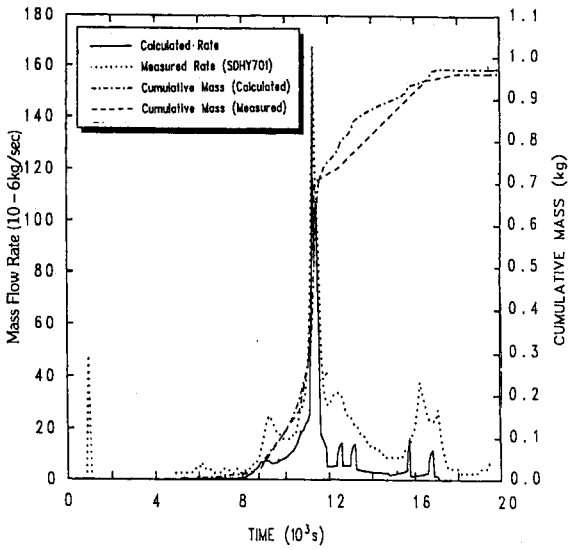

Fig. 12. Production Rate and Cumulative Mass of Hydrogen

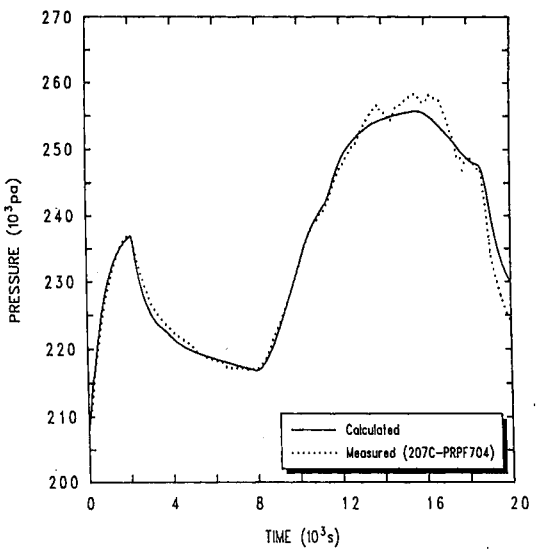

Fig. 13. Pressure in the Containment

agreement with 96 g in the experiment [14]. The period with a high hydrogen production rate takes place between 11,100 and 11,600 sec. The timing and duration of the period agree well with the experimental observation.

Fuel relocation : According to the degradation criteria, the oxidized zircaloy cladding (ZrO_2) is sufficiently strong to hold-up the fuel pellets until 2,500 K. At 15,560 sec, the fuel in cell 213 (second ring, level 13) starts to melt and relocate.

The calculated timing of the fuel movement is good agreement with the experimental data of 15,800 sec. But all fuel relocation in the calculation (about 5 %) differs from the experiment which was terminated when about 20 % of the fuel is degraded. The under predicted fuel relocation in the calculation reflects the fact that the fuel relocation is considered only melting but not debris formation.

Control rod poison : The control rod is heated indirectly by the high temperature fuel rods nearby, through radiation and convection. At 10,649 sec, the Ag-In-Cd control rod poison starts melting. The molten Ag-In-Cd is located outside the control rod tube as conglomerate debris, and it can candle downward to colder regions where it solidifies. If the temperature increases in this region, the conglomerate debris melts again, and candles progress further downward.

Containment behavior : Steam and hydrogen that is produced during the oxidation reaction inside the core, enter the containment vessel and determine the thermal-hydraulic behavior. Fission products enter the containment vessel along with the gas flow. The behavior of the fission product is described in section 4.2.

The steam mass flow into the containment is different from the core inlet as shown in Fig. 6. There is a dip in the mass flow rate at the core outlet at about 11,200 sec, caused by the oxidation reaction in the core in which steam reacts with zircaloy and steel, and hydrogen is

Table 3. Mass (kg) distribution of radioactive nuclide at 20000 sec.

Class	Initial inventory	Core (fuel)	Deposition in RCS			Containment			Release fraction (%)
			core	hot leg	SG	airborne	deposit*	total	
1. Xe	3.784E-2	6.594E-3	0.000E-0	0.000E-0	0.000E-0	3.121E-2	0.000E-0	3.121E-2	82.58
2. Cs	1.736E-2	3.033E-3	1.556E-4	6.297E-9	6.438E-3	1.931E-3	4.701E-3	6.632E-3	81.32
3. Ba	1.578E-2	1.201E-2	5.834E-5	2.405E-3	6.241E-4	3.429E-4	3.375E-4	6.804E-4	23.87
4. I	1.318E-3	2.304E-4	-	-	-	-	-	-	82.54
5. Te	2.992E-3	2.180E-3	8.448E-6	0.419E-9	3.875E-4	1.844E-4	2.307E-4	4.151E-4	27.12
6. Ru	1.859E-2	1.842E-2	3.289E-5	5.664E-5	4.150E-5	2.408E-5	2.141E-5	4.549E-5	0.948
7. Mo	2.550E-2	2.155E-2	6.741E-4	1.281E-3	9.450E-4	4.657E-4	5.479E-3	1.041E-3	15.37
8. Ce	3.906E-2	3.906E-2	6.784E-7	3.361E-6	2.473E-6	1.375E-6	1.321E-6	2.696E-6	0.024
9. La	4.906E-2	4.905E-2	2.097E-6	9.180E-6	6.763E-6	4.205E-6	3.332E-6	7.538E-6	0.053
10. U	9.375E-0	9.374E-0	6.656E-4	1.115E-3	8.194E-4	5.035E-4	4.084E-4	9.120E-4	0.037
11. Cd	2.378E-4	1.087E-4	3.171E-6	5.231E-5	3.535E-5	1.844E-5	1.977E-5	3.821E-5	54.28
12. Sn	6.166E-4	3.907E-4	8.205E-6	8.270E-5	6.486E-5	3.355E-5	3.649E-5	7.004E-5	36.62
16. CsI	1.000E-6	1.000E-6	1.745E-5	1.102E-9	1.077E-3	3.303E-4	8.006E-4	1.131E-3	-

* deposit means the sum of the aerosol in the pool and the aerosol deposited on the structures

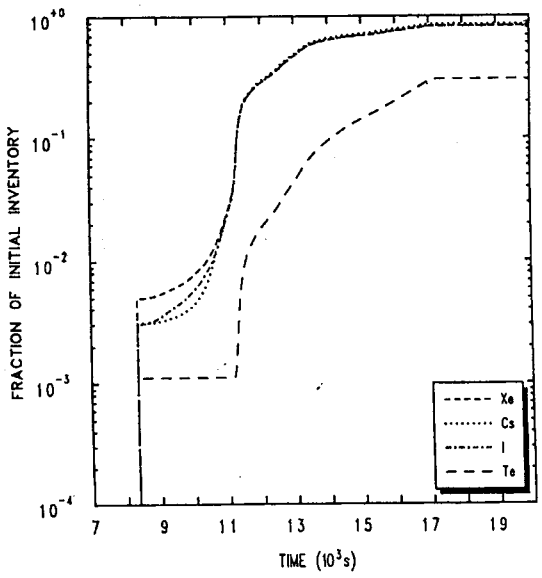

Fig. 14. Cumulative Release Fraction of Volatile Compounds from the Fuel (class 1,2,5, 16)

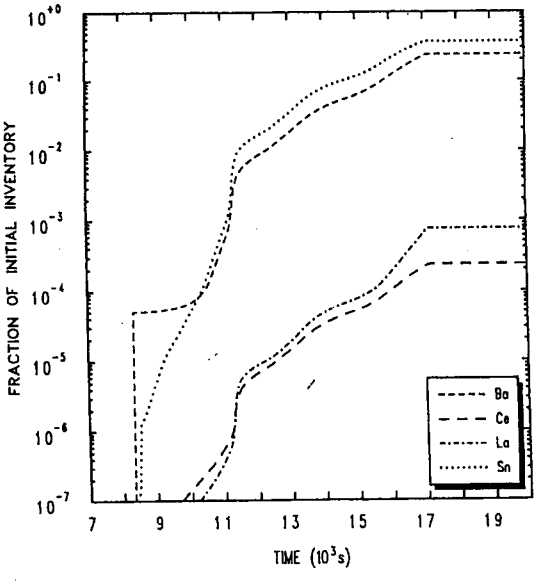

Fig. 15. Cumulative Release Fraction of Non-volatile Compounds from the Fuel. (class 3.8.9.12)

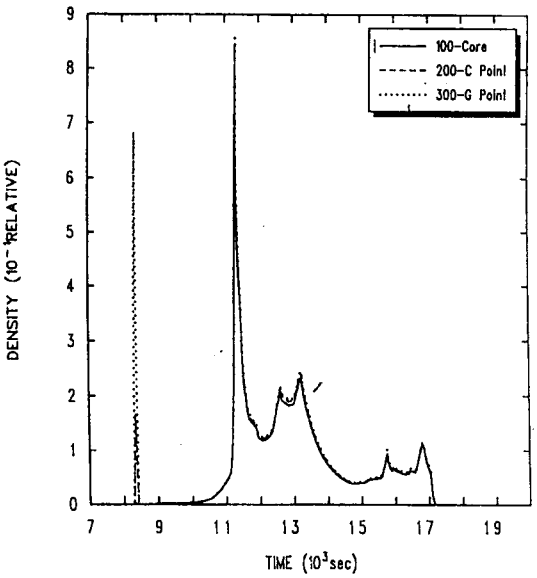

Fig. 16. Distribution of Relative Mass of Xe (noble gas) Along the Primary Circuit

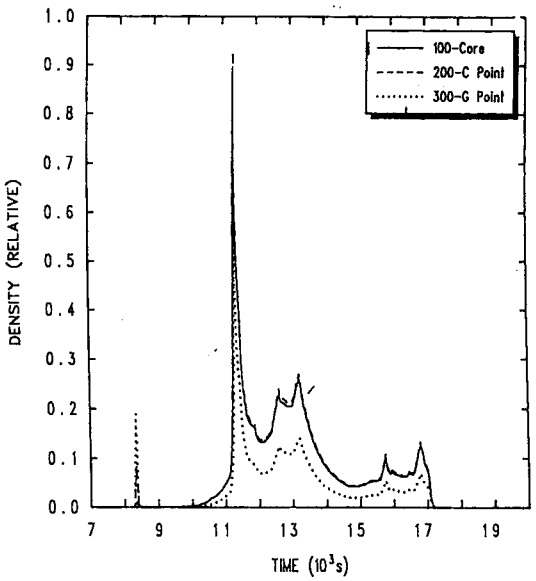

Fig. 17. Distribution of Relative Mass of Cs (volatile component) Along the Primary Circuit

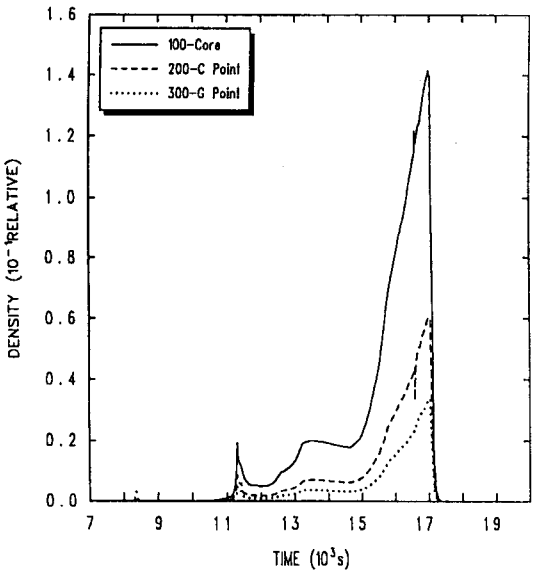

Fig. 18. Distribution of Relative Mass of Ba (less-volatile component) Along the Primary Circuit

formed. Most of the steam introduced into the containment vessel condenses on the three condensers. If the steam mass flow increases, the steam builds up in the vessel and the pressure increases until an equilibrium pressure is reached at which the steam condensation rate equals to the steam mass flow rate into the vessel. Reversely, the pressure decreases, if the steam mass flow decreases. The calculated containment pressure agrees well with the experiment as shown in Fig. 13.

4.2. Fission Product Behavior

Fission product release from the bundle :

During the degradation of the core, fission products are released from the core. The experimental results concerning fission product release, however, are currently not available. The

initial core inventory and the mass release from the core at the end of the calculation at 20,000 sec are presented in Table 3 for all MELCOR classes. The cumulative release fractions from the fuel are shown in Figs. 14 and 15. Fig. 14 shows the classes with volatile components (noble gases, Cs, I, Te), while the classes shown in Fig. 15 are less- or non-volatile components (Ba, Ce, La, Sn).

In this calculation, the volatile fission products in MELCOR classes 1, 2, 3, 4 and 5 are assumed to be subject to gap release. Note that I (class 4) immediately recombines with Cs (class 2) to form CsI (class 16). The release rate of volatile fission products shows a sharp and high peak at the initial gap release at 8,333 sec (see Figs. 16 and 17). The gap release of less- volatile Ba is very small in Fig. 18. Note also that these figures give the sum of the aerosol and vapor concentration in the primary circuit, and the history of core concen-tration is the same as the release rate since the fluid velocity is high enough. The larger part of the fission product release occurs due to the fuel heat-up.

For the control rod poison behavior, the CORSOR release model is applied. According to the CORSOR model, release only takes place at temperatures above 1,173 K, and the release rate is increased at higher temperatures. In the calculation, the control rod poison melts at 1,075 K, and candles downward to colder regions. Since the melting temperature is below the minimum temperature for release, the control rod poison release is predicted very small.

Fission product behavior in the circuit : Fission products that are released from the core flow through the primary circuit. The main emphasis will be on the concentration and deposition at points C and G, where the two instrumentation groups are located. The deposition of all classes are given in Table 3. On the basis of deposition behavior, the classes can roughly be divided into three groups.

The first group consists only of the noble gases (class 1), which do not deposit in the primary circuit. Fig. 16 show the sum of the aerosol and vapor concentration in the gas phase at core, point C, and point G for the noble gases. As shown in Fig. 16, relative mass density in the atmosphere are same in the primary circuit. Therefore, all noble gases that are released from the core are transported to the containment vessel without deposition.

The second group consists of the volatile components; classes 2 (Cs), 5 (Te), and 16 (CsI). The main deposition mechanism for these classes is condensation. As shown in Fig. 17, relative mass density at point C is the same as at the core, but at point G is much lower. These classes do not deposit in the hot part of the primary circuit, because they are in the gaseous form. If the wall temperature is sufficiently low, the vapors of these classes condense and deposition takes place. The deposition starts in the steam generator U-tube. Cs is deposited in the first part of the vertical pipe within a short time period of gap release, but revaporized soon. A fraction of about 50 % of the released mass from the core is deposited in the primary circuit. The remaining fraction is transported to the containment vessel as aerosols.

The third group consists of less- and non-volatile components; classes 3, 6 through 12. As shown in Fig. 18, relative mass density at point C is lower than the value at the core, and at point G is lower than at point C. The main deposition mechanism for these classes is thermophoresis. Consequently, these classes show a high deposition in the hot part of the circuit (shroud, upper plenum, and riser), as well as in the first part of the steam generator. A fraction of about 65 % (40 % in hot part and 25 % in SG) of the released mass from the core is deposited in the

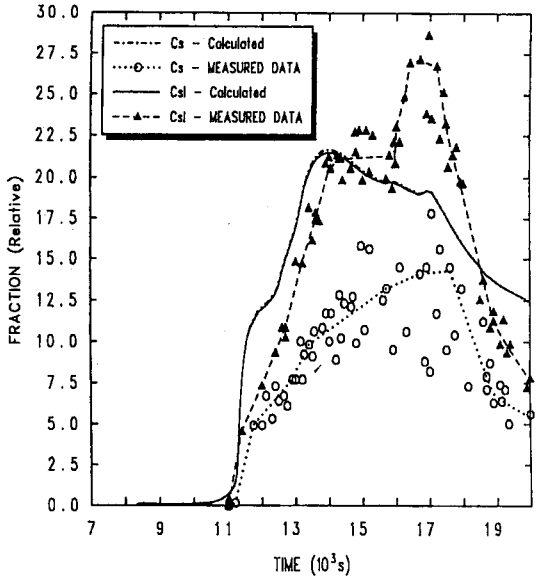

Fig. 19. Aerosol Concentration in the Gas Phase of the Containment for Class 2 and 16

primary circuit. The remaining 35 % is transported to the containment vessel as aerosols.

Fission product behavior in the containment:

Fig. 19 show the sum of the aerosol and vapor concentration in the gas phase of the containment vessel for MELCOR classes 2 (Cs) and 16 (CsI) with experimental data.

Immediately after the gap release at 8,333 sec, the concentrations of the volatile species in the containment vessel are very low and the aerosol flow into the containment is negligible during the next 2,000 sec. The fission product release due to fuel heat-up starts at about 10,000 sec and aerosol flow rate into the containment shows a peak at about 11,300 sec as shown in Fig. 17.

From 11,000 sec, agglomeration starts to play an important role, because the concentration of aerosols in the containment have increased considerably. As a consequence, the aerosol size and the deposition rate increase. After fuel melting and relocation at about 16,000 sec, the measured aerosol concentration increases, but calculated concentration decrease continually due to the inadequate release model in the molten pool.

The fission product release from the core stops after the power shutdown at 17,040 sec, but aerosol deposition is continued. Therefore, the aerosol concentration in the containment decrease until the calculation terminate. The calculated removal rate is lower than that from the experiment, which is mainly because the hygroscopic model is not applied in this calculation.

The calculation extends over a period of 20,000 sec. At the end of this period, a significant fraction of the aerosols is still airborne. These airborne aerosols will deposit during the subsequent experimental phases that follow the degradation phase. The deposition behavior after 20,000 sec is not performed in this simulation.

5. Summary of Main Results

This paper describes the results of the PHEBUS FPT1 post test analysis that has been performed with MELCOR computer code, version 1.8.4. A comparison of calculated results with experimental data has been made for the thermal-hydraulic behavior of the test bundle and the containment, and it is found that the simulation using MELCOR code shows good agreement with the experiment. But the result of fission product behavior could not be compared with the experiment, because no information of fission product behavior is available yet.

Thermal hydraulic behavior

- The calculated cladding rupture time is much later than in the experiment, but the rupture temperature is predicted very well. The delayed predicted rupture time resulted in since the fuel

temperature is almost constant in the range from 4,500 sec to 8000 sec during the thermal calibration phase

- The calculated starting time of the fuel degradation shows good agreement with the experiment, but the extent of the fuel damage is predicted smaller than occurred in the experiment (5% versus 20%). The reason of the small mass of fuel relocation in the calculation is that fuel relocation occurred only by melting but not debris formation.
- The total calculated hydrogen production is 97 g, which agrees well with the experiment (96 g). The timing and duration of the oxidation runaway also agree with the experiment.
- During the calculational period, the thermal hydraulic behavior of the containment showed good agreement with the experiment.
- For the fuel relocation model option, it is better to allow that the fuel rod is held within oxidized zircaloy.

Fission product behavior

- The CORSOR release model in MELCOR code has been used for the fuel release, but no experimental data is available for comparison.
- A reasonable result of fission product release can be obtained by the CORSOR release model from the fuel. But there is no adequate model for the release from the molten fuel and control rod, so the CORSOR release model is also applied. Therefore, the released mass of the Ag-In-Cd control rod poison is underpredicted, and fission product release from the molten fuel about 16,000 sec is also small.
- The aerosol concentration in the containment without hygroscopic model is predicted higher than the experimental value. the hygroscopic model, therefore, has to be applied for the aerosol behavior in the containment.
- The volatile components, which do not deposit in the hot part of the primary circuit, start to deposit in the steam generator. A fraction of about 50 % of the released mass form the core deposits in the primary circuit.
- Less-volatile and non-volatile components show a high deposition in the hot part of the circuit, as well as in the first part of the steam generator. A fraction of about 65% of the released mass from the core deposits in the primary circuit.
- At the end of the calculational period, a significant fraction of the aerosols is still airborne. These airborne aerosols will deposit during the subsequent experiment.

Reference

1. B.Berthet, et al., "PHEBUS FP ; FPT1-Preliminary Report," Notes Tech. LERES No 24/97, Doc. PHEBUS PF IP/97/334, Oct. (1997).
2. M.Swartz and A.Jones, "FPT1 Test Definition : Objectives and Status Revison 3," Note Tech. SEMAR 93/91, SAWG 91-017/3, CPF064 Rev3 (1993).
3. R.M.Summers, et al., "MELCOR Computer Code Manuals," SNL, NUREG/CR-6119, SAND93-2185, Sep. (1994).
4. W.Krischer and M.C.Rubinstein, "The PHEBUS Fission Product Project," Elsevier Applied Science, (1992).
5. P.Von Der Hardt and A.Tattergain, "The PHEBUS Fission Product Project," J. of Nucl. Mat., 188, p115, (1992).
6. N.Hanniet and G.Repetto, "FPT0 Final Report," IPSN/DRS/SEA/ LERES/97/1815, Cadarache, Dec., (1997).
7. Marc Vandegehuehte, private communication (experimental data).
8. H.Scheurer, "PHEBUS FP Data Book FPT1," IS-92-49, CEA, JRC, Mar.(1995).

9. S.Bourdon, et al., "Final Test Protocol for the PHEBUS FP Test FPT1," Note Tech. SEMAR 96/61, May (1996).
10. M.C.Ribinstein, "Minutes of the 27th SAWG Meeting held in Aix-en-Provence," MCR/MJ 20/10/97, IPSN, Sep. 24, (1997).
11. B.Berthet, "Quantitative Analyses of the FPT1 Tomographies," Note Tech. LERES 57/97, Dec., (1997).
12. M.R.Kuhlman, et al., "CORSOR User's Manual," NUREG/CR-4173, BMI-2122, (1985).
13. USNRC, "Technical Bases for Estimating Fission Product Behavior During LWR Accident," NUREG-0772, June (1981).
14. C.Martin, "Hydrogen Production during the FPT1 TEST - Analysis of the Experimental Results," Notes Tech. LERES No 4/97, Doc. PHEBUS PF IP/97/341, Sep. (1997).